

Differential cross section measurement of charged current ν_e interactions without final-state pions in MicroBooNE

P. Abratenko,³⁴ J. Anthony,⁴ L. Arellano,¹⁹ J. Asaadi,³³ A. Ashkenazi,³¹ S. Balasubramanian,¹¹ B. Baller,¹¹ C. Barnes,²¹ G. Barr,²⁴ J. Barrow,^{20,31} V. Basque,¹¹ L. Bathe-Peters,¹³ O. Benevides Rodrigues,³⁰ S. Berkman,¹¹ A. Bhandari,¹⁹ M. Bhattacharya,¹¹ M. Bishai,² A. Blake,¹⁶ B. Bogart,²¹ T. Bolton,¹⁵ J. Y. Book,¹³ L. Camilleri,⁹ D. Caratelli,³ I. Caro Terrazas,⁸ F. Cavanna,¹¹ G. Cerati,¹¹ Y. Chen,²⁷ J. M. Conrad,²⁰ M. Convery,²⁷ L. Cooper-Troendle,³⁷ J. I. Crespo-Anadón,⁵ M. Del Tutto,¹¹ S. R. Dennis,⁴ P. Detje,⁴ A. Devitt,¹⁶ R. Diurba,^{1,22} R. Dorrill,¹⁴ K. Duffy,²⁴ S. Dytman,²⁵ B. Eberly,²⁹ A. Ereditato,¹ J. J. Evans,¹⁹ R. Fine,¹⁷ O. G. Finnerud,¹⁹ W. Foreman,¹⁴ B. T. Fleming,³⁷ N. Foppiani,¹³ D. Franco,³⁷ A. P. Furmanski,²² D. Garcia-Gomez,¹² S. Gardiner,¹¹ G. Ge,⁹ S. Gollapinni,^{32,17} O. Goodwin,¹⁹ E. Gramellini,¹¹ P. Green,¹⁹ H. Greenlee,¹¹ W. Gu,² R. Guenette,¹⁹ P. Guzowski,¹⁹ L. Hagaman,³⁷ O. Hen,²⁰ R. Hicks,¹⁷ C. Hilgenberg,²² G. A. Horton-Smith,¹⁵ B. Irwin,²² R. Itay,²⁷ C. James,¹¹ X. Ji,² L. Jiang,³⁵ J. H. Jo,³⁷ R. A. Johnson,⁷ Y.-J. Jwa,⁹ D. Kalra,⁹ N. Kamp,²⁰ G. Karagiorgi,⁹ W. Ketchum,¹¹ M. Kirby,¹¹ T. Kobilarcik,¹¹ I. Kreslo,¹ M. B. Leibovitch,³ I. Lepetic,²⁶ J.-Y. Li,¹⁰ K. Li,³⁷ Y. Li,² K. Lin,²⁶ B. R. Littlejohn,¹⁴ W. C. Louis,¹⁷ X. Luo,³ K. Manivannan,³⁰ C. Mariani,³⁵ D. Marsden,¹⁹ J. Marshall,³⁶ D. A. Martinez Caicedo,²⁸ K. Mason,³⁴ A. Mastbaum,²⁶ N. McConkey,¹⁹ V. Meddage,¹⁵ K. Miller,⁶ J. Mills,³⁴ A. Mogan,⁸ T. Mohayai,¹¹ M. Mooney,⁸ A. F. Moor,⁴ C. D. Moore,¹¹ L. Mora Lepin,¹⁹ J. Mousseau,²¹ S. Mullerlababu,¹ D. Naples,²⁵ A. Navrer-Agasson,¹⁹ N. Nayak,² M. Nebot-Guinot,¹⁰ D. A. Newmark,¹⁷ J. Nowak,¹⁶ M. Nunes,³⁰ N. Oza,¹⁷ O. Palamara,¹¹ N. Pallat,²² V. Paolone,²⁵ A. Papadopoulou,²⁰ V. Papavassiliou,²³ H. B. Parkinson,¹⁰ S. F. Pate,²³ N. Patel,¹⁶ Z. Pavlovic,¹¹ E. Piasetzky,³¹ I. D. Ponce-Pinto,³⁷ S. Prince,¹³ X. Qian,² J. L. Raaf,¹¹ V. Radeka,² M. Reggiani-Guzzo,¹⁹ L. Ren,²³ L. Rochester,²⁷ J. Rodriguez Rondon,²⁸ M. Rosenberg,³⁴ M. Ross-Lonergan,^{9,17} C. Rudolf von Rohr,¹ G. Scanavini,³⁷ D. W. Schmitz,⁶ A. Schukraft,¹¹ W. Seligman,⁹ M. H. Shaevitz,⁹ R. Sharankova,¹¹ J. Shi,⁴ A. Smith,⁴ E. L. Snider,¹¹ M. Soderberg,³⁰ S. Söldner-Rembold,¹⁹ J. Spitz,²¹ M. Stancari,¹¹ J. St. John,¹¹ T. Strauss,¹¹ S. Sword-Fehlberg,²³ A. M. Szec,¹⁰ W. Tang,³² N. Taniuchi,⁴ K. Terao,²⁷ C. Thorpe,¹⁶ D. Torbunov,² D. Totani,³ M. Toups,¹¹ Y.-T. Tsai,²⁷ J. Tyler,¹⁵ M. A. Uchida,⁴ T. Usher,²⁷ B. Viren,² M. Weber,¹ H. Wei,¹⁸ A. J. White,³⁷ Z. Williams,³³ S. Wolbers,¹¹ T. Wongjirad,³⁴ M. Wospakrik,¹¹ K. Wresilo,⁴ N. Wright,²⁰ W. Wu,¹¹ E. Yandel,³ T. Yang,¹¹ L. E. Yates,¹¹ H. W. Yu,² G. P. Zeller,¹¹ J. Zennamo,¹¹ and C. Zhang²

(The MicroBooNE Collaboration)*

¹Universität Bern, Bern CH-3012, Switzerland

²Brookhaven National Laboratory (BNL), Upton, NY, 11973, USA

³University of California, Santa Barbara, CA, 93106, USA

⁴University of Cambridge, Cambridge CB3 0HE, United Kingdom

⁵Centro de Investigaciones Energéticas, Medioambientales y Tecnológicas (CIEMAT), Madrid E-28040, Spain

⁶University of Chicago, Chicago, IL, 60637, USA

⁷University of Cincinnati, Cincinnati, OH, 45221, USA

⁸Colorado State University, Fort Collins, CO, 80523, USA

⁹Columbia University, New York, NY, 10027, USA

¹⁰University of Edinburgh, Edinburgh EH9 3FD, United Kingdom

¹¹Fermi National Accelerator Laboratory (FNAL), Batavia, IL 60510, USA

¹²Universidad de Granada, Granada E-18071, Spain

¹³Harvard University, Cambridge, MA 02138, USA

¹⁴Illinois Institute of Technology (IIT), Chicago, IL 60616, USA

¹⁵Kansas State University (KSU), Manhattan, KS, 66506, USA

¹⁶Lancaster University, Lancaster LA1 4YW, United Kingdom

¹⁷Los Alamos National Laboratory (LANL), Los Alamos, NM, 87545, USA

¹⁸Louisiana State University, Baton Rouge, LA, 70803, USA

¹⁹The University of Manchester, Manchester M13 9PL, United Kingdom

²⁰Massachusetts Institute of Technology (MIT), Cambridge, MA, 02139, USA

²¹University of Michigan, Ann Arbor, MI, 48109, USA

²²University of Minnesota, Minneapolis, MN, 55455, USA

²³New Mexico State University (NMSU), Las Cruces, NM, 88003, USA

²⁴University of Oxford, Oxford OX1 3RH, United Kingdom

²⁵University of Pittsburgh, Pittsburgh, PA, 15260, USA

²⁶Rutgers University, Piscataway, NJ, 08854, USA

²⁷SLAC National Accelerator Laboratory, Menlo Park, CA, 94025, USA

²⁸South Dakota School of Mines and Technology (SDSMT), Rapid City, SD, 57701, USA

²⁹University of Southern Maine, Portland, ME, 04104, USA

³⁰*Syracuse University, Syracuse, NY, 13244, USA*

³¹*Tel Aviv University, Tel Aviv, Israel, 69978*

³²*University of Tennessee, Knoxville, TN, 37996, USA*

³³*University of Texas, Arlington, TX, 76019, USA*

³⁴*Tufts University, Medford, MA, 02155, USA*

³⁵*Center for Neutrino Physics, Virginia Tech, Blacksburg, VA, 24061, USA*

³⁶*University of Warwick, Coventry CV4 7AL, United Kingdom*

³⁷*Wright Laboratory, Department of Physics, Yale University, New Haven, CT, 06520, USA*

(Dated: August 5, 2022)

In this letter we present the first measurements of an exclusive electron neutrino cross section with the MicroBooNE experiment using data from the Booster Neutrino Beamline at Fermilab. These measurements are made for a selection of charged-current electron neutrinos without final-state pions. Differential cross sections are extracted in energy and angle with respect to the beam for the electron and the leading proton. The differential cross section as a function of proton energy is measured using events with protons both above and below the visibility threshold. This is done by including a separate selection of electron neutrino events without reconstructed proton candidates in addition to those with proton candidates. Results are compared to the predictions from several modern generators, and we find the data agrees well with these models. The data shows best agreement, as quantified by p -value, with the generators that predict a lower overall cross section, such as GENIE v3 and NuWro.

Many fundamental questions in neutrino physics are still unresolved [1] and will be addressed by upcoming experiments that use liquid argon detectors [2, 3]. These experiments will look for the appearance of electron neutrinos in a muon-neutrino beam to search for CP violation, measure the neutrino mass ordering, and explore longstanding anomalies. They will also address broader physics goals such as searching for dark matter particles in the beam, for which ν_e interactions are a dominant background, and characterizing supernova explosions, for which ν_e interactions are the primary signal. It is therefore vital to improve the modeling of ν_e interactions in argon to enable those searches with high sensitivity.

We present a measurement of ν_e interactions in argon without final-state pions in MicroBooNE, both with and without visible protons. This analysis is the first ν_e -argon cross section measurement in an exclusive final state and provides additional model discrimination relative to previous inclusive measurements. Also, as a first ν_e cross section measurement on the Booster Neutrino Beamline (BNB) [4] at Fermilab, we provide a complementary result to previous measurements on argon [5–7] performed on ν_e events from the Neutrinos at the Main Injector (NuMI) beamline [8]. This measurement also complements the differential electron neutrino cross-section measurement on a hydrocarbon target in a similar exclusive final state [9].

MicroBooNE has recently completed the first round of searches [10–13] for an excess of low-energy charged-current (CC) ν_e interactions that could explain the MiniBooNE anomaly [14], and did not observe an excess. The search for ν_e events without visible final-state pions [11], however, observed mild tension with the model used to predict the ν_e interaction rate. Consistency was found

to be at the 10%–20% level in terms of p -values after systematic uncertainties were constrained with a high-statistics measurement of CC ν_μ interactions from the same beam. In this letter we build on this result to perform a cross section measurement under the assumption of no new physics, with the goal of providing input to neutrino interaction model development.

The MicroBooNE detector [15] is a liquid argon time projection chamber (TPC). The TPC is a 2.56 m by 2.32 m by 10.36 m volume filled with 85 metric tons of liquid argon. As charged particles travel through the detector, they ionize the argon, and the ionization electrons drift in the applied electric field of 273 V/cm, to be detected by induction on two planes of wires and collected on the third plane of wires. Each plane of wires has a different orientation (vertical, $+60^\circ$, -60°) so that when they are read out in time they result in three different “views” that are combined to derive 3D images of neutrino interactions. The detector also contains a light collection system, consisting of 32 photomultiplier tubes with fast timing resolution, that makes it possible to identify ionization electrons coincident with the neutrino beam arrival.

The neutrinos measured in this analysis come from the BNB. They have an average energy of about 0.8 GeV and are primarily muon neutrinos, with only a 0.5% contribution from electron neutrinos [16]. This analysis measures this intrinsic electron neutrino component using data collected from 2016–2018, corresponding to 6.86×10^{20} protons on target (POT).

The neutrino flux simulation used in this analysis was developed by the MiniBooNE collaboration [16] and is modified to use the position of MicroBooNE. Neutrino interactions in the detector argon are simulated using v3.0.6 G18_10a_02_11a of the GENIE event generator [17] with the MicroBooNE tune applied [18]. There are several steps involved to simulate the detector response. Particles are propagated through the detector us-

* microboone_info@fnal.gov

ing Geant4 [19], and then the charge and light produced by these particles is simulated with LArSoft [20]. A simulation of the charge induced by drifting electrons is used for the wire and readout electronics response [21, 22]. Scintillation light propagation is modeled with a look-up table from a Geant4 simulation of photon propagation. Data-driven electric field maps are used to take into account distortions in the electric field from space charge [23, 24]. Ion recombination is simulated with a modified box model [25], and a time dependent simulation is used for the drift electron lifetime and wire response. Cosmic rays are a significant background in MicroBooNE and are incorporated in a data-driven way by overlaying a simulated neutrino interaction onto cosmic data collected during periods of time when the neutrino beam was off. This method also provides a data-driven incorporation of detector noise.

Neutrino events are reconstructed in this analysis using the Pandora pattern-recognition toolkit [26]. A set of algorithms first removes obvious cosmic-rays that cross the detector and then selects a neutrino candidate in time with the beam. Particles are reconstructed as showers or tracks within this neutrino candidate; typically electrons and photons are shower-like, while muons, charged pions, and protons are track-like. The Pandora event reconstruction has been used for many previously published results by the MicroBooNE collaboration [6, 7, 11, 27–34]. Additional tools are used on top of the Pandora pattern recognition to enhance shower-track separation, perform particle identification to separate proton and muon tracks [35], and to perform electron-photon separation for showers [11]. Track and shower energies are measured separately. Calorimetric energy reconstruction is performed for electromagnetic showers starting with the total energy clustered in the shower (E_{shr}). This is corrected to account for inefficiencies in charge collection using a simulation of electrons and with this correction the reconstructed energy is defined as $E_{\text{reco}}=E_{\text{shr}}/0.83$. For tracks, the energy is estimated based on particle range [36]. Using simulation, the energy resolution is estimated to be 3% for protons if their kinetic energy (KE) is greater than 50 MeV, and 12% for electrons. The absolute resolution on $\cos\theta$ is 0.01 for electrons and 0.03 for protons, where θ is the angle of the particle with respect to the beam.

We define true signal events as charged current ν_e interactions that contain an outgoing electron with $\text{KE}_e > 30$ MeV, and do not contain final-state charged pions with $\text{KE}_{\pi^\pm} > 40$ MeV or any neutral pions. Signal events are further characterized in terms of the leading proton kinetic energy. Events with visible protons ($\text{KE}_p \geq 50$ MeV) are defined as $1eNp0\pi$ events. Events without visible protons ($\text{KE}_p < 50$ MeV), or events for which no proton exits the nucleus, are defined as $1e0p0\pi$ events [37]. These $1e0p0\pi$ events are required to pass additional phase space restrictions on the electron energy ($E_e > 0.5$ GeV) and the angle between the neutrino beam and electron directions ($\cos\theta_e > 0.6$).

We perform a differential cross section measurement in four kinematic variables: the electron energy, the electron angle with respect to the beam, the leading proton energy, and the leading proton angle with respect to the beam. All of these variables except the leading proton energy are measured for only the $1eNp0\pi$ signal. The leading proton energy measurement includes both $1e0p0\pi$ and $1eNp0\pi$ events with smearing allowed between these two samples. This is possible because $1e0p0\pi$ signal events by definition have a leading proton kinetic energy below 50 MeV, and therefore these events can be included as a single bin in the proton kinetic energy measurement from 0 to 50 MeV. This is the first measurement to characterize proton production in neutrino interactions across the visibility threshold. Using the MicroBooNE tune of GENIE v3 [18], $1eNp0\pi$ events are predicted to be 60% quasi-elastic (QE) neutrino interactions, 30% meson exchange current (MEC), and with subdominant contributions from resonant (RES) (10%) and deep inelastic scattering (DIS) (1%) interactions; $1e0p0\pi$ events are mostly QE, with contributions from MEC and RES each at the 10%–15% level [37]. The relative abundance of the different interaction types is not flat with respect to the measured variables which may provide some insight into the differences between models when data is compared to event generators.

Events are selected with separate criteria based on the presence or absence of candidate protons. This selection strategy is the same as in Ref. [11], although a few of the requirements have been updated to optimize the selections for a cross section measurement. The main objective is to maintain sufficient ν_e purity for a cross-section extraction while maximizing the ν_e efficiency across the phase space of the measurement. For both the $1eNp0\pi$ and $1e0p0\pi$ selections the largest increase in efficiency comes from a relaxed cut on the boosted decision trees (BDTs) used in the analysis. These BDTs are the same, including the training, as those used in Ref. [11]. Additionally, for the $1eNp0\pi$ selection, we relax the requirements on proton vs muon particle identification, on the shower dE/dx , and on the shower conversion distance. For the $1e0p0\pi$ selection we add requirements to increase the purity as needed for a cross-section measurement, particularly on the energy deposited per unit length (dE/dx) at the start of the electron candidate, and by restricting the phase space to the highest-purity region with $\cos\theta_e^{\text{reco}} > 0.6$ and $E_e^{\text{reco}} > 0.51$ GeV. We find that with these selections an appropriate visibility threshold for the leading proton kinetic energy is 50 MeV, which is approximately where the $1e0p0\pi$ selection efficiency turns off and the $1eNp0\pi$ efficiency turns on [37]. Therefore, for $1eNp0\pi$ selected events we also require that the leading reconstructed proton has $\text{KE}_p^{\text{reco}} > 50$ MeV.

With the data sample used in this analysis, a total of 145.5 events are predicted in the $1eNp0\pi$ selection, with a $1eNp0\pi$ purity of 69%. We expect to select about 100 (2) true $1eNp0\pi$ ($1e0p0\pi$) events with an efficiency of 17%. The largest backgrounds to the $1eNp0\pi$ selection

are events with final state π^0 (ν_e CC and ν_μ CC or NC interactions, for a total 15.3 predicted events), other ν_μ CC events (12.9 predicted events), and cosmic rays (6.8 predicted events). In the $1e0p0\pi$ selection about 10 (2) true $1e0p0\pi$ ($1eNp0\pi$) signal events are predicted with an efficiency of 12% and $1e0p0\pi$ purity of 65%; the total prediction is 17.6 events, and the largest background is from interactions with final state π^0 mesons (2.8 predicted events).

The prediction on the total number of selected events is subject to uncertainties from several sources. Variations in the flux prediction may come from uncertainties on the hadron production cross section and on the modeling of the beamline [16, 38]. These are propagated to an uncertainty on the predicted event rate by reweighting the nominal simulation, and are found to be at the 6% level and mostly flat in terms of the variables used in the analysis. Uncertainties on the neutrino interaction model are included based on the nominal tuned GENIE v3 simulation using a reweighting method for most of the sources and with a limited set of specific variations [18]. The impact of the interaction model uncertainties is only evaluated on the efficiency and smearing for true signal events; the number of signal events is not varied as it is the quantity of interest for the cross-section measurement. These combine to a 4% uncertainty on the total event prediction. Uncertainties on the propagation of final state particles in the detector are assessed by varying re-interaction cross sections for charged pions and protons, again by reweighting [39]. These uncertainties are generally at the 1% level, but grow to as high as 8% at high proton energies. Uncertainties on detector modeling are assessed using dedicated samples that are produced by varying parameters related to specific detector effects to amounts compatible with estimates from MicroBooNE data. These include space-charge effects, electron-ion recombination, light measurement, and wire response [40]. Overall, these effects combine to approximately a 5% effect but can grow to 10%–20% at high electron and proton energies as well as for the $1e0p0\pi$ selection. Other subdominant uncertainties are due to the size of simulated samples, the POT measurement, and the estimate of the total number of argon nuclei in the detector.

Covariance matrix formalism is used to include systematic uncertainties in the analysis, where the total systematic uncertainty covariance matrix C^{Syst} is defined as the sum of the covariance matrices of each uncertainty (flux, cross section, re-interaction, detector, Monte Carlo statistics, POT, and the number of nuclei), with individual entries written as C_{ij} :

$$C_{ij} = \frac{1}{N} \sum_{k=1}^N \left(n_i^k - n_i^{\text{CV}} \right) \left(n_j^k - n_j^{\text{CV}} \right). \quad (1)$$

Here the covariance matrix is written in terms of bin indices i and j , and constructed as a sum over systematic variations k up until the total number of systematic variations N , with the central value bin content defined as

n^{CV} and the content of bin i in variation k defined as n_i^k . Finally, statistical uncertainties from the data measurement are included as

$$C^{\text{Tot}} = C^{\text{Syst}} + C^{\text{DataStat}}, \quad (2)$$

where C^{DataStat} is diagonal with elements corresponding to the Poisson variance in each bin. Statistical uncertainties in the data are the leading source of uncertainty in this measurement.

The observed distributions for the four variables considered in this analysis are shown in Fig. 1, where the data is overlaid on top of the nominal simulation based on the tuned version of GENIE v3 [18]. The data sample consists of 111 events selected with the $1eNp0\pi$ selection and an additional 14 events with the $1e0p0\pi$ selection. The simulation predicts more events than the data, especially at forward angles with respect to the beam and at intermediate energies. These are similar observations to those presented in Ref. [11].

To extract the cross section from the observed number of events we first define a response matrix, which maps the generated signal events in the true variable space to the observed signal events after selection in the reconstructed space. The off-diagonal elements of the response matrix define the amount of smearing between true and reconstructed bins. Both $1e0p0\pi$ and $1eNp0\pi$ events are included in the response matrix for the proton energy, with $1e0p0\pi$ events in a single bin and $1eNp0\pi$ events in the other bins. This means that smearing is included between these selections through the off-diagonal elements. The other variables use only $1eNp0\pi$ events. Due to the limited size of the selected data sample the bin width is typically larger than the resolution on the measured variables so smearing is limited and most events fall into the correct bins with >70% across all variables and >90% for electron angle. An unfolded differential cross-section measurement in the true-space bin i for the variable x measured in reconstructed-space bin j is defined as:

$$\left\langle \frac{d\sigma}{dx} \right\rangle_i = \frac{\sum_j U_{ij}(n_j - b_j)}{N_{\text{target}} \times \phi \times (\Delta x)_i}, \quad (3)$$

where U is the unfolding matrix, n is the number of data events, b is the number of background events, N_{target} is the number of nucleons, ϕ is the integrated electron neutrino flux, and $(\Delta x)_i$ is the measured bin width in the variable x . The unfolding matrix U is used in place of the inverse of the response matrix R^{-1} to avoid instabilities in the cross-section result from a direct matrix inversion. We extract the cross section using an unfolding procedure based on the D'Agostini method [41] with three iterations. This number of iterations is found to give results that are stable and with limited bin-to-bin fluctuations. In the cross-section extraction, we use a number of nucleons equal to 4.3912×10^{31} , and a POT-integrated BNB ν_e flux of $2.73 \times 10^9 \text{ cm}^{-2}$, which is taken to be the reference flux [42] of the measurement and used as a constant value. As described in a previous MicroBooNE publication [43], this method allows for a consistent treatment

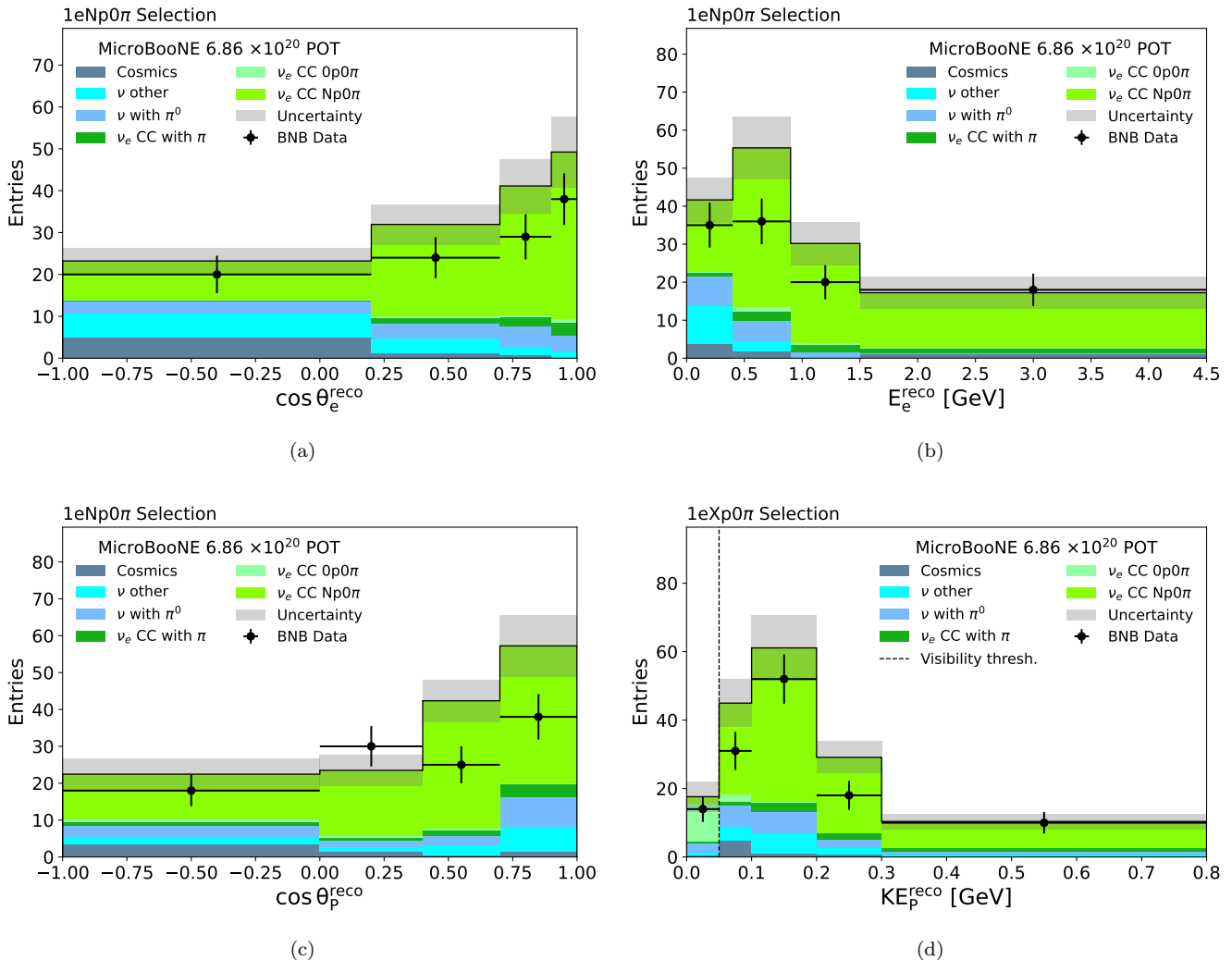


FIG. 1. The observed number of events in data compared to the simulated prediction using the MicroBooNE tune of GENIE v3. The selection used is reported in each panel. The $1eNp0\pi$ selection is used for (a) the angle between the neutrino beam and electron direction, (b) the electron energy, and (c) the angle between the neutrino beam and leading proton direction. The $1eXp0\pi = (1e0p0\pi \text{ OR } 1eNp0\pi)$ selection is used for (d), the leading proton kinetic energy, where events selected with the $1e0p0\pi$ selection populate the leftmost bin and events from the $1eNp0\pi$ selection populate the other bins.

of flux uncertainties. The uncertainties on the total prediction (Eq. 2) are analytically propagated through the unfolding procedure to obtain a covariance matrix in unfolded cross section [44].

The resulting cross sections are presented in Fig. 2, where they are compared to a number of modern generators: the MicroBooNE tune of GENIE v3.0.6 [18], GENIE v3.0.6 G18_10a_02_11a [17], GENIE v2.12.2 [45, 46], NuWro 19.02.1 [47, 48], and NEUT v5.4.0 [49, 50]. These generators have different initial state nuclear models (GENIE v2 uses a relativistic Fermi gas, while the others use a local Fermi gas), quasi-elastic models (GENIE v3 and NEUT use Valencia [51–53], GENIE v2 and NuWro use Llewellyn Smith [54]), and MEC models (GENIE v2 uses an empirical model, and the others the Valencia model). Details about the models used

in these generators and a more complete description of their differences are found in other MicroBooNE publications [7, 28, 29] and a summary table presented in [55]. We assess the agreement with these generators by computing χ^2 values and the p -values corresponding to the upper tail of the cumulative distribution for the χ^2 per degrees of freedom.

While all generators are in reasonable agreement with the data, the level of agreement differs depending on the generator and the variable as shown in Table I. The data indicate a preference for GENIE v3 and NuWro, both of which have a smaller overall electron neutrino prediction. Compared to the default GENIE v3, the MicroBooNE tune enhances the QE and MEC components and tends to over-predict, especially at intermediate energies. The lowest p -values are obtained for NEUT, which predicts

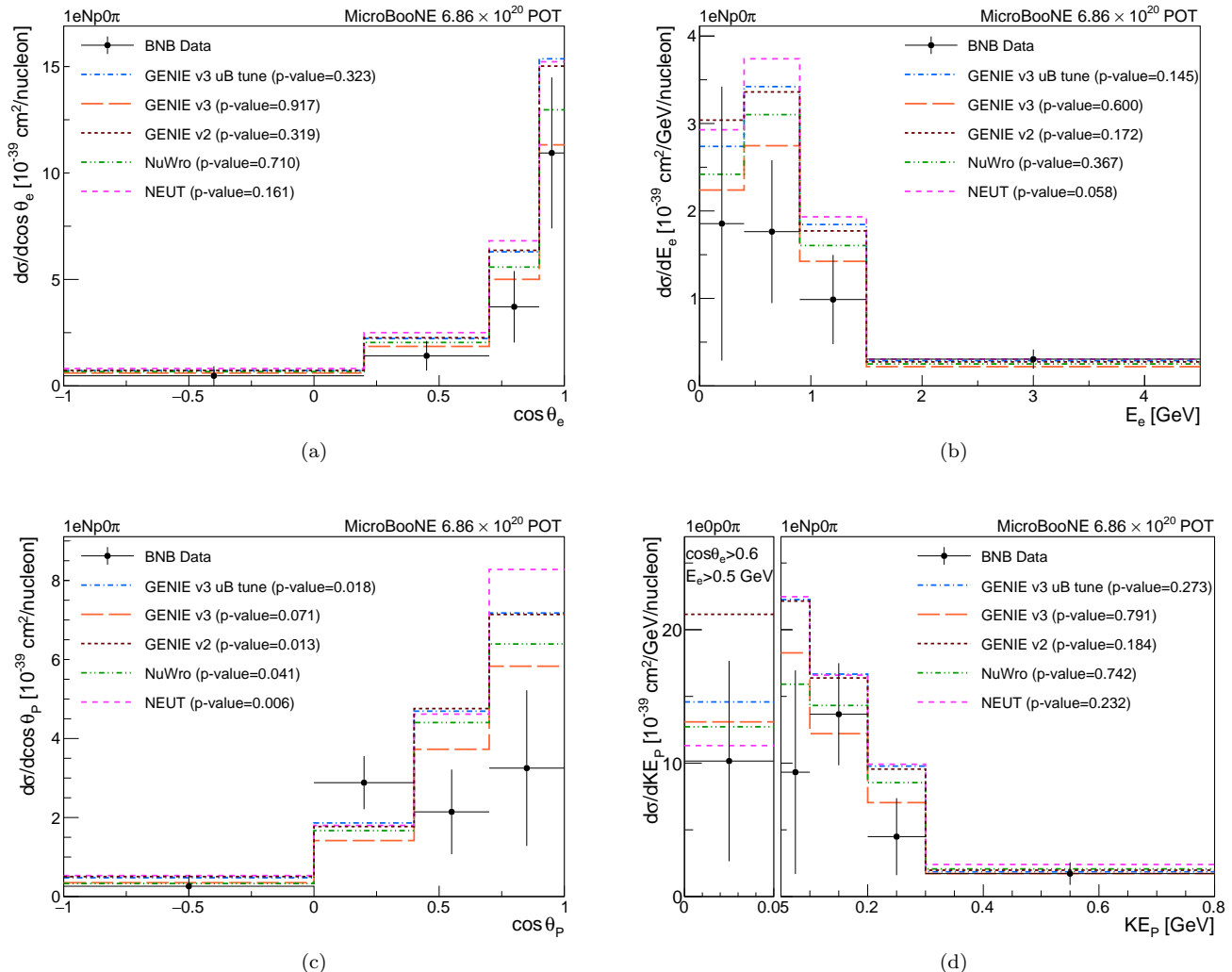


FIG. 2. Differential cross sections from unfolded data and comparisons with predictions from different generators. The signal definition is reported for each panel: $1eNp0\pi$ is used for (a) the angle between the neutrino beam and electron direction, (b) the electron energy, (c) the angle between the neutrino beam and the leading proton direction, and the right panel of (d) the leading proton kinetic energy. An additional phase space restriction is applied to the leftmost panel of (d). Compatibility is evaluated in terms of p -values, and reported in the legends.

TABLE I. Agreement between unfolded data and generator neutrino interaction models represented as p -values.

Generator	$\cos \theta_e$	E_e	$\cos \theta_p$	KE_p
GENIE v3 uB tune	0.323	0.145	0.018	0.273
GENIE v3	0.917	0.600	0.071	0.791
GENIE v2	0.319	0.172	0.013	0.184
NuWro	0.710	0.367	0.041	0.742
NEUT	0.161	0.058	0.006	0.232

the largest overall cross section, especially at forward proton angles, and GENIE v2, which has the largest prediction for $1e0p0\pi$ events, partly due to its empirical MEC model [56] with no Pauli blocking. The discrepancy between data and generator models is largest

in leading proton angle, with p -values that range from 1% to 7%, and is most pronounced in the forward direction. Future measurements with more statistics will be able to further explore these features. More information about these results is provided in supplementary material, including tabulated cross-section values, χ^2 values, the background-subtracted observations, covariance matrices, and response matrices [37].

In summary, this letter presents the first differential ν_e -argon cross-section measurement without pions in the final state in electron angle and energy as well as leading proton angle and energy, where the proton energy is characterized both above and below the visibility threshold. The findings are typically in agreement with predictions from modern generators, except for tension in the proton

angle, with an overall preference for those with lower total cross section. These results provide input for further tuning of generators towards an improved ν_e prediction for future new-physics searches in MicroBooNE, SBN [3], and DUNE [57]. While this result is statistically limited, an approximately equivalent data set from later run periods remains to be analyzed and can be used, in addition to possible reconstruction and selection improvements, for future cross-section measurements.

This document was prepared by the MicroBooNE collaboration using the resources of the Fermi National Accelerator Laboratory (Fermilab), a U.S. Department of Energy, Office of Science, HEP User Facility. Fermilab is managed by Fermi Research Alliance, LLC (FRA), acting under Contract No. DE-AC02-07CH11359. MicroBooNE is supported by the following: the U.S. Department of Energy, Office of Science, Offices of High Energy Physics and Nuclear Physics; the U.S.

National Science Foundation; the Swiss National Science Foundation; the Science and Technology Facilities Council (STFC), part of the United Kingdom Research and Innovation; the Royal Society (United Kingdom); and the UK Research and Innovation (UKRI) Future Leaders Fellowship. Additional support for the laser calibration system and cosmic ray tagger was provided by the Albert Einstein Center for Fundamental Physics, Bern, Switzerland. We also acknowledge the contributions of technical and scientific staff to the design, construction, and operation of the MicroBooNE detector as well as the contributions of past collaborators to the development of MicroBooNE analyses, without whom this work would not have been possible. For the purpose of open access, the authors have applied a Creative Commons Attribution (CC BY) public copyright license to any Author Accepted Manuscript version arising from this submission.

-
- [1] M. Sajjad Athar *et al.*, “Status and perspectives of neutrino physics,” *Prog. Part. Nucl. Phys.* **124**, 103947 (2022).
- [2] B. Abi *et al.* (DUNE Collaboration), “Deep Underground Neutrino Experiment (DUNE), Far Detector Technical Design Report, Volume II: DUNE Physics,” [arXiv:2002.03005](https://arxiv.org/abs/2002.03005) [hep-ex].
- [3] M. Antonello *et al.* (MicroBooNE, LAr1-ND, ICARUS-WA104 Collaborations), “A Proposal for a Three Detector Short-Baseline Neutrino Oscillation Program in the Fermilab Booster Neutrino Beam,” [arXiv:1503.01520](https://arxiv.org/abs/1503.01520) [physics.ins-det].
- [4] I. Stancu, “Technical Design Report for the 8 GeV Beam,” [FERMILAB-DESIGN-2001-03](https://arxiv.org/abs/2001.10217) (2001), 10.2172/1212167.
- [5] R. Acciarri *et al.* (ArgoNeuT Collaboration), “First measurement of electron neutrino scattering cross section on argon,” *Phys. Rev. D* **102**, 011101 (2020).
- [6] P. Abratenko *et al.* (MicroBooNE Collaboration), “Measurement of the flux-averaged inclusive charged-current electron neutrino and antineutrino cross section on argon using the NuMI beam and the MicroBooNE detector,” *Phys. Rev. D* **104**, 052002 (2021).
- [7] P. Abratenko *et al.* (MicroBooNE Collaboration), “First measurement of inclusive electron-neutrino and antineutrino charged current differential cross sections in charged lepton energy on argon in MicroBooNE,” *Phys. Rev. D* **105**, L051102 (2022).
- [8] P. Adamson *et al.*, “The NuMI Neutrino Beam,” *Nucl. Instrum. Meth. A* **806**, 279–306 (2016).
- [9] J. Wolcott *et al.* (MINERvA Collaboration), “Measurement of electron neutrino quasielastic and quasielasticlike scattering on hydrocarbon at $\langle E_\nu \rangle = 3.6$ GeV,” *Phys. Rev. Lett.* **116**, 081802 (2016).
- [10] P. Abratenko *et al.* (MicroBooNE Collaboration), “Search for an Excess of Electron Neutrino Interactions in MicroBooNE Using Multiple Final-State Topologies,” *Phys. Rev. Lett.* **128**, 241801 (2022).
- [11] P. Abratenko *et al.* (MicroBooNE Collaboration), “Search for an anomalous excess of charged-current ν_e interactions without pions in the final state with the MicroBooNE experiment,” *Phys. Rev. D* **105**, 112004 (2022).
- [12] P. Abratenko *et al.* (MicroBooNE Collaboration), “Search for an anomalous excess of charged-current quasielastic ν_e interactions with the MicroBooNE experiment using Deep-Learning-based reconstruction,” *Phys. Rev. D* **105**, 112003 (2022).
- [13] P. Abratenko *et al.* (MicroBooNE Collaboration), “Search for an anomalous excess of inclusive charged-current ν_e interactions in the MicroBooNE experiment using Wire-Cell reconstruction,” *Phys. Rev. D* **105**, 112005 (2022).
- [14] A. A. Aguilar-Arevalo *et al.* (MiniBooNE Collaboration), “Updated MiniBooNE neutrino oscillation results with increased data and new background studies,” *Phys. Rev. D* **103**, 052002 (2021).
- [15] R. Acciarri *et al.* (MicroBooNE Collaboration), “Design and Construction of the MicroBooNE Detector,” *J. Instrum.* **12**, P02017 (2017).
- [16] A. A. Aguilar-Arevalo *et al.* (MiniBooNE Collaboration), “The Neutrino Flux prediction at MiniBooNE,” *Phys. Rev. D* **79**, 072002 (2009).
- [17] L. Alvarez-Ruso *et al.* (GENIE Collaboration), “Recent highlights from GENIE v3,” *Eur. Phys. J. ST* **230**, 4449–4467 (2021).
- [18] P. Abratenko *et al.* (MicroBooNE Collaboration), “New $CC0\pi$ GENIE model tune for MicroBooNE,” *Phys. Rev. D* **105**, 072001 (2022).
- [19] S. Agostinelli *et al.* (Geant4 Collaboration), “GEANT4—a simulation toolkit,” *Nucl. Instrum. Meth. A* **506**, 250–303 (2003).
- [20] E. L. Snider and G. Petrillo, “LArSoft: Toolkit for Simulation, Reconstruction and Analysis of Liquid Argon TPC Neutrino Detectors,” *J. Phys. Conf. Ser.* **898**, 042057 (2017).
- [21] C. Adams *et al.* (MicroBooNE Collaboration), “Ionization electron signal processing in single phase LArTPCs. Part I. Algorithm Description and quantitative evaluation with MicroBooNE simulation,” *J. Instrum.* **13**,

- P07006 (2018).
- [22] C. Adams *et al.* (MicroBooNE Collaboration), “Ionization electron signal processing in single phase LArTPCs. Part II. Data/simulation comparison and performance in MicroBooNE,” *J. Instrum.* **13**, P07007 (2018).
- [23] C. Adams *et al.* (MicroBooNE Collaboration), “A method to determine the electric field of liquid argon time projection chambers using a UV laser system and its application in MicroBooNE,” *J. Instrum.* **15**, P07010 (2020).
- [24] P. Abratenko *et al.* (MicroBooNE Collaboration), “Measurement of space charge effects in the MicroBooNE LArTPC using cosmic muons,” *J. Instrum.* **15**, P12037 (2020).
- [25] R. Acciarri *et al.* (ArgoNeuT Collaboration), “A Study of Electron Recombination Using Highly Ionizing Particles in the ArgoNeuT Liquid Argon TPC,” *J. Instrum.* **8**, P08005 (2013).
- [26] R. Acciarri *et al.* (MicroBooNE Collaboration), “The Pandora multi-algorithm approach to automated pattern recognition of cosmic-ray muon and neutrino events in the MicroBooNE detector,” *Eur. Phys. J. C* **78**, 82 (2018).
- [27] P. Abratenko *et al.* (MicroBooNE Collaboration), “Search for Neutrino-Induced Neutral-Current Δ Radiative Decay in MicroBooNE and a First Test of the MiniBooNE Low Energy Excess under a Single-Photon Hypothesis,” *Phys. Rev. Lett.* **128**, 111801 (2022).
- [28] P. Abratenko *et al.* (MicroBooNE Collaboration), “Measurement of differential cross sections for ν_μ -Ar charged-current interactions with protons and no pions in the final state with the MicroBooNE detector,” *Phys. Rev. D* **102**, 112013 (2020).
- [29] P. Abratenko *et al.* (MicroBooNE Collaboration), “First Measurement of Differential Charged Current Quasielastic-like ν_μ -Argon Scattering Cross Sections with the MicroBooNE Detector,” *Phys. Rev. Lett.* **125**, 201803 (2020).
- [30] P. Abratenko *et al.* (MicroBooNE Collaboration), “First Measurement of Inclusive Muon Neutrino Charged Current Differential Cross Sections on Argon at $E_\nu \sim 0.8$ GeV with the MicroBooNE Detector,” *Phys. Rev. Lett.* **123**, 131801 (2019).
- [31] C. Adams *et al.* (MicroBooNE Collaboration), “First measurement of ν_μ charged-current π^0 production on argon with the MicroBooNE detector,” *Phys. Rev. D* **99**, 091102 (2019).
- [32] C. Adams *et al.* (MicroBooNE Collaboration), “Comparison of ν_μ -Ar multiplicity distributions observed by MicroBooNE to GENIE model predictions,” *Eur. Phys. J. C* **79**, 248 (2019).
- [33] P. Abratenko *et al.* (MicroBooNE Collaboration), “Search for a Higgs Portal Scalar Decaying to Electron-Positron Pairs in the MicroBooNE Detector,” *Phys. Rev. Lett.* **127**, 151803 (2021).
- [34] P. Abratenko *et al.* (MicroBooNE Collaboration), “Search for Heavy Neutral Leptons Decaying into Muon-Pion Pairs in the MicroBooNE Detector,” *Phys. Rev. D* **101**, 052001 (2020).
- [35] P. Abratenko *et al.* (MicroBooNE Collaboration), “Calorimetric classification of track-like signatures in liquid argon TPCs using MicroBooNE data,” *J. High Energy Phys.* **12**, 153 (2021).
- [36] M. Berger, J. Coursey, and M. Zucker, “ESTAR, PSTAR, and ASTAR: Computer Programs for Calculating Stopping-Power and Range Tables for Electrons, Protons, and Helium Ions (version 1.21),” (1999) <http://physics.nist.gov/Star>.
- [37] P. Abratenko *et al.* (MicroBooNE Collaboration), Supplemental Material at [URL will be inserted by publisher].
- [38] A. A. Aguilar-Arevalo *et al.* (MiniBooNE Collaboration), “Improved Search for $\bar{\nu}_\mu \rightarrow \bar{\nu}_e$ Oscillations in the MiniBooNE Experiment,” *Phys. Rev. Lett.* **110**, 161801 (2013).
- [39] J. Calcutt, C. Thorpe, K. Mahn, and L. Fields, “Geant4Reweight: a framework for evaluating and propagating hadronic interaction uncertainties in Geant4,” *J. Instrum.* **16**, P08042 (2021).
- [40] P. Abratenko *et al.* (MicroBooNE Collaboration), “Novel approach for evaluating detector-related uncertainties in a LArTPC using MicroBooNE data,” *Eur. Phys. J. C* **82**, 454 (2022).
- [41] G. D’Agostini, “Improved iterative bayesian unfolding,” [arXiv:1010.0632](https://arxiv.org/abs/1010.0632).
- [42] L. Koch and S. Dolan, “Treatment of flux shape uncertainties in unfolded, flux-averaged neutrino cross-section measurements,” *Phys. Rev. D* **102**, 113012 (2020).
- [43] P. Abratenko *et al.* (MicroBooNE Collaboration), “First Measurement of Energy-Dependent Inclusive Muon Neutrino Charged-Current Cross Sections on Argon with the MicroBooNE Detector,” *Phys. Rev. Lett.* **128**, 151801 (2022).
- [44] J. Bourbeau and Z. Hampel-Arias, “PyUnfold: A Python Package for Iterative Unfolding,” (2018), [10.5281/zenodo.1258211](https://arxiv.org/abs/10.5281/zenodo.1258211), [arXiv:1806.03350](https://arxiv.org/abs/1806.03350) [physics.data-an].
- [45] C. Andreopoulos *et al.*, “The GENIE Neutrino Monte Carlo Generator,” *Nucl. Instrum. Meth. A* **614**, 87–104 (2010).
- [46] C. Andreopoulos, C. Barry, S. Dytman, H. Gallagher, T. Golan, R. Hatcher, G. Perdue, and J. Yarba, “The GENIE Neutrino Monte Carlo Generator: Physics and User Manual,” [arXiv:1510.05494](https://arxiv.org/abs/1510.05494) [hep-ph].
- [47] T. Golan, J. T. Sobczyk, and J. Zmuda, “NuWro: the Wroclaw Monte Carlo Generator of Neutrino Interactions,” *Nucl. Phys. B Proc. Suppl.* **229-232**, 499–499 (2012).
- [48] T. Golan, C. Juszczak, and J. T. Sobczyk, “Final State Interactions Effects in Neutrino-Nucleus Interactions,” *Phys. Rev. C* **86**, 015505 (2012).
- [49] Y. Hayato, “A neutrino interaction simulation program library NEUT,” *Acta Phys. Polon. B* **40**, 2477–2489 (2009).
- [50] Y. Hayato and L. Pickering, “The NEUT neutrino interaction simulation program library,” *Eur. Phys. J. ST* **230**, 4469–4481 (2021).
- [51] J. Nieves, I. Ruiz Simo, and M. J. Vicente Vacas, “Inclusive Charged-Current Neutrino-Nucleus Reactions,” *Phys. Rev. C* **83**, 045501 (2011).
- [52] J. Schwehr, D. Cherdack, and R. Gran, “GENIE implementation of IFIC Valencia model for QE-like 2p2h neutrino-nucleus cross section,” [arXiv:1601.02038](https://arxiv.org/abs/1601.02038) [hep-ph].
- [53] R. Gran, J. Nieves, F. Sanchez, and M. J. Vicente Vacas, “Neutrino-nucleus quasi-elastic and 2p2h interactions up to 10 GeV,” *Phys. Rev. D* **88**, 113007 (2013).
- [54] C. H. Llewellyn Smith, “Neutrino Reactions at Accelerator Energies,” *Phys. Rept.* **3**, 261–379 (1972).

- [55] D. Doyle *et al.* (NOvA Collaboration), “Measurement of the Double-Differential Muon-neutrino Charged-Current Inclusive Cross Section in the NOvA Near Detector,” [arXiv:2109.12220](https://arxiv.org/abs/2109.12220) [hep-ex].
- [56] T. Katori, “Meson Exchange Current (MEC) Models in Neutrino Interaction Generators,” *AIP Conf. Proc.* **1663**, 030001 (2015).
- [57] B. Abi *et al.* (DUNE Collaboration), “Prospects for beyond the Standard Model physics searches at the Deep Underground Neutrino Experiment,” *Eur. Phys. J. C* **81**, 322 (2021).